Astronomy & Astrophysics manuscript no. gd1_mepp
June 12, 2023

Modelling the formation of the GD-1 stellar stream inside a host with a fermionic dark matter core-halo distribution.

Martín F. Mestre[1,2,⋆], Carlos R. Argüelles[1,2], and Daniel D. Carpintero[1,2]

[1] Instituto de Astrofísica de La Plata (CONICET-UNLP), Paseo del Bosque S/N, La Plata (1900), Buenos Aires, Argentina

[2] Facultad de Ciencias Astronómicas y Geofísicas de La Plata (UNLP), Paseo del Bosque S/N, La Plata (1900), Buenos Aires, Argentina

Received February 29, 2023; accepted February 30, 2023

ABSTRACT

Context. Stellar streams are a consequence of the tidal forces produced by a host galaxy on its satellites (i.e. globular clusters and dwarf spheroidals). As the self-gravity of stellar streams is almost negligible, they constitute excellent probes of the gravitational potential of the host galaxy. For this reason, some Milky Way stellar streams have been used to put constraints on the dark matter (DM) total mass and shape, under empirical DM distributions (i.e. NFW, logarithmic, etc). Within the set of non-empirical DM distributions, there exists a DM model deduced from first principles by means of the maximization of the coarse-grained entropy for self-gravitating fermions, the MEPP, after Maximum Entropy Production Principle. MEPP profiles have a rich variety of behaviours, being a large subfamily characterized by a dense core of mass $\approx 4.1 \times 10^6 M_\odot$ (that can mimick a black hole regarding the orbits of the S-stars at Sagittario A*) and an extended halo with the plasticity of a Burkert profile.
Aims. In this work we attempt to model the GD-1 stellar stream using a spherical MEPP distribution which, at the same time, is in sintony with previous fits to the S-stars.
Methods. For that purpose we used a genetic algorithm in order to fit both the stream orbit's initial conditions and the fermionic halo. We modelled the barionic potential with a bulge and two disks (thin and thick) with fixed parameters according to the recent literature. The stream observable is 6D phase-space data from the Gaia DR2 survey.
Results. We were able to find good fits for a 1D continuous subfamily of models parametrized by the fermion mass going from 56 keV/c^2 to 360 keV/c^2, respectively corresponding to core radii going from 10^3 to 10 Schwarzschild radii. For smaller and larger values of the fermion mass, there is no solution that simultaneously fits the GD-1 stream and the S-stars. The solutions have a virial radius of 28 kpc and a virial mass of $1.4 \times 10^{11} M_\odot$, the latter being at 2σ from previous Milky Way DM halo mass estimates using the Sagittarius stream. We do not assume the velocity of the local standard of rest ($v_{\rm lsr}$) and the result gives $v_{\rm lsr} \approx 244$ km/s, in agreement with recent independent estimates.

Key words. Galaxy: kinematics and dynamics – Galaxy: stellar streams – dark matter

1. Introduction

Stellar streams probe the acceleration field produced by the Milky Way (MW). This information together with barionic measurements help in making claims about the dark matter halo.

2. Methodology

In this section we explain the observables and methods used in this research.

2.1. Observables and assumed measurements

The main observables used in this project are materialized by the polynomial fits performed by Ibata et al. (2020) on the GD-1 stream using astrometry (Gaia DR2), photometry and high-precision spectroscopy datasets together with the analysis of the STREAMFINDER algorithm. Those polinomials are the following:

$$\phi_2 = 0.008367\phi_1^3 - 0.05332\phi_1^2 - 0.07739\phi_1 - 0.02007, \quad (1)$$

$$D = -4.302\phi_1^5 - 11.54\phi_1^4 - 7.161\phi_1^3 + 5.985\phi_1^2 + 8.595\phi_1 + 10.36, \quad (2)$$

$$\tilde{\mu}_\alpha = 3.794\phi_1^3 + 9.467\phi_1^2 + 1.615\phi_1 - 7.844, \quad (3)$$

$$\mu_\delta = -1.225\phi_1^3 + 8.313\phi_1^2 + 18.68\phi_1 - 3.95, \quad (4)$$

$$v_h = 90.68\phi_1^3 + 204.5\phi_1^2 - 254.2\phi_1 - 261.5, \quad (5)$$

$$(6)$$

with ϕ_1 and ϕ_2 in radians, D in kpc, $\tilde{\mu}_\alpha = \mu_\alpha cos\delta$ and μ_δ in mas/yr and v_h in km/s. These quantities correspond respectively to longitude and latitude in GD-1 celestial frame of reference (Koposov et al. 2010), heliocentric distance, proper motion in right ascension and declination, and heliocentric radial velocity. The domain of this polinomials is limited to $-90 < \phi_1[^\circ] < 10$. To have our observable data points we sample the domain with 100 points ($\phi_1^{(i)}$ for $i = 1, ..., 100$) and evaluate the polinomials there in order to have a complete set of observables ($\phi_1^{(i)}$, $\phi_2^{(i)}$, $D^{(i)}$, $\tilde{\mu}_\alpha^{(i)}$, $\mu_\delta^{(i)}$, $v_h^{(i)}$). In one of the experiments we will consider

⋆ e-mail: mmestre@fcaglp.unlp.edu.ar

an observable of a different nature and related to the density concentration at the origin, of size $\lesssim 1$ milliparsec, characteristic of the fermionic halo distribution. By convention, the core radius is defined as the radius when the circular velocity reaches its first maximum. The constraint for the mass of the core of the distribution is assumed to be $m_{\rm core} = 3.5 \times 10^6 M_\odot$ in agreement with Becerra-Vergara et al. (2020, 2021); Argüelles et al. (2022).

The assumed measurements used in this paper are the galactocentric distance of the sun $R_\odot = 8.122$ kpc (GRAVITY Collaboration et al. 2018) and the sun's peculiar velocity $\boldsymbol{v}_{\odot p} = (11.1, 12.24, 7.25)$ km/s (Schönrich et al. 2010).

2.2. The fermionic dark matter model

Our dark matter model consists of a spherical and isotropic distribution of fermions at finite temperature in hydrostatic equilibrium subject to the law of General Relativity (i.e. T.O.V equations) as defined in Argüelles et al. (2018) with the particularity that we have made a few change of variables in order to make the numerical computation more robust. The system of equations thus obtained is as follows:

$$\frac{d\nu}{d\zeta} = \frac{1}{2}\left[e^z + e^{2\zeta}\frac{P(r)}{\rho_{rel}c^2}\right][1-e^z]^{-1}, \tag{7}$$

$$\frac{dz}{d\zeta} = -1 + e^{(2\zeta - z)}\frac{\rho(r)}{\rho_{rel}}, \tag{8}$$

where

$$\zeta = \ln(r/R), \tag{9}$$

$$z = \ln\psi, \quad \psi = \frac{M_{\rm DM}(r)}{M}\frac{R}{r}, \tag{10}$$

$$\rho(r) = \frac{4\rho_{\rm rel}}{\sqrt{\pi}}\int_1^\infty \epsilon^2[\epsilon^2-1]^{1/2} f(r,\epsilon)d\epsilon, \tag{11}$$

$$P(r) = \frac{4\rho_{\rm rel}c^2}{3\sqrt{\pi}}\int_1^\infty [\epsilon^2-1]^{3/2} f(r,\epsilon)d\epsilon, \tag{12}$$

$$R^2 = \frac{c^2}{8\pi G\rho_{\rm rel}}, \tag{13}$$

$$M = 4\pi R^3 \rho_{\rm rel}, \tag{14}$$

$$\rho_{\rm rel} = \frac{G\pi^{3/2}m^4c^3}{h^3}, \tag{15}$$

where G is the Gravitational constant, c is the speed of light, h is the Planck constant, m is the fermion mass, $M_{\rm DM}(r)$ is dark matter mass enclosed up to radius r, $\rho(r)$ is the density, $P(r)$ is the pressure and $\nu(r)$ is the metric exponent, i.e. we use the convention $g_{00} = e^{\nu(r)}$. The phase-space function (f) is given by a Fermi-Dirac distribution with energy cutoff:

$$f(r,\epsilon) = \begin{cases} \dfrac{1-e^{[\epsilon-\epsilon_c(r)]/\beta(r)}}{1+e^{[\epsilon-\alpha(r)]/\beta(r)}} & \epsilon \le \epsilon_c(r) \\ 0 \quad \epsilon > \epsilon_c(r), \end{cases} \tag{16}$$

where $\alpha(r)$ is the chemical potential (including rest mass), $\epsilon_c(r)$ is the cutoff energy (including rest mass) and $\beta(r)$ is the temperature variable.

The above equations should be complemented with two thermodinamic equilibrium conditions given in Tolman (1930) and Klein (1949) together with the condition of energy conservation along the geodesic given in Merafina & Ruffini (1989):

$$\frac{1}{\alpha}\frac{d\alpha}{dr} = \frac{1}{\beta}\frac{d\beta}{dr} = \frac{1}{\epsilon_c}\frac{d\epsilon_c}{dr} = -\frac{1}{2}\frac{d\nu}{dr}. \tag{17}$$

It is not possible to integrate this equations from $r = 0$ because the right hand the change of variables $\zeta(r)$ is divergent at the origin. Nevertheless, it is possible to reach the following approximations for the initial conditions at a value $r_{\rm min} \gtrsim 0$:

$$\nu(r_{\rm min}) \approx \frac{1}{6}\frac{\rho_0}{\rho_{\rm rel}}\left[\frac{r_{\rm min}}{R}\right]^2 \equiv \tau, \tag{18}$$

$$\psi(r_{\rm min}) \approx \frac{1}{3}\frac{\rho_0}{\rho_{\rm rel}}\left[\frac{r_{\rm min}}{R}\right]^2 = 2\tau, \tag{19}$$

which implies

$$\frac{r_{\rm min}}{R} = \sqrt{6\tau\frac{\rho_{\rm rel}}{\rho_0}}, \tag{20}$$

where $\rho_0 \equiv \rho(0)$. It can be seen that the right hand side of Eq. 7 does not depend on the metric so we can add a constant ν_0 to the solution in order to satisfy a condition of continuity with the Schwarzschild metric at the border of the fermion distribution, obtaining:

$$\nu_0 = 2\ln\left(\frac{\beta_b}{\beta_0}\sqrt{1-\psi_b}\right),$$

where ψ_b and β_b are quantities evaluated at the border.

The system of equations thus obtained has four free parameters: m, $\alpha_0 = \alpha(0)$, $\beta_0 = \beta(0)$, and $\epsilon_{c0} = \epsilon_c(0)$ but in practice we will use the following related quantities as parameters: m, β_0, $\theta_0 = (\alpha_0 - 1)/\beta_0$, and $W_0 = (\epsilon_{c0} - 1)/\beta_0$.

Equations 7-17 are solved using a Python (Van Rossum & Drake Jr 1995) script[1] that makes use of the NumPy (Virtanen et al. 2020) and SciPy (Harris et al. 2020) packages. We tried all the solvers available in the latter package but the only one that could properly integrate these equations was the `LSODA` algorithm. We used relative and absolute tolerance parameters respectively given by `rtol`$= 5 \times 10^{-14}$ and `atol`$= 0$.

2.3. Milky Way and stream models

We model our Galaxy with a combination of the fermionic dark halo recently described, whose parameters will be determined in this work, plus a barionic component fixed and identical to the one in Model I of Pouliasis et al. (2017). Here we name this full Galaxy model as Fermionic-MW.

Appart from our model, for some intermediary tasks, we will make use of the Galactic model fitted by Malhan & Ibata (2019) which consists in the `MWPotential2014` model with an axisymmetric NFW profile. This fitted model corresponds to a circular velocity at the position of the sun of $v_c(R_\odot) = 244 \pm 4 \mathrm{kms}^{-1}$ and a $z-$flattening of the dark matter density distribution of $q_\rho = 0.82^{+0.25}_{-0.13}$. Here we name this Galaxy model as NFW-MW.

As GD-1 is a dynamically cold stream, with its stars keeping a large degree of correlation, its almost one-dimensional distribution in phase-space can be well approximated with the orbit of its progenitor. Another facts in this direction, are that there has not been any observation of the tidal arms feature nor of the progenitor's position (Malhan & Ibata 2019; de Boer et al. 2018; Malhan et al. 2018; Price-Whelan & Bonaca 2018).

In the code, the orbit model is computed starting from initial conditions in spherical equatorial coordinates, ICRS frame: α (RA), δ (declination), D, $\tilde{\mu}_\alpha$, μ_δ, v_h. The code uses the Astropy ecosystem (Astropy Collaboration et al. 2022, 2018, 2013) in

[1] https://github.com/martinmestre/stream-fit/blob/main/likelihood_grid/optim/model_def.py

order to transform the initial condition to galactocentric coordinates assuming a Galactocentric reference frame with the sun at the position $\boldsymbol{x}_\odot = (-R_\odot, 0, 0)$ and a sun's velocity given by the sum of the circular velocity at the position of the sun and the sun's peculiar velocity: $\boldsymbol{v}_\odot = (11.1, v_c(R_\odot) + 12.24, 7.25)$. The circular velocity is dependent on the model and the position and given by

$$\begin{aligned} v_c^2(R_\odot) &= R_\odot \|\nabla\Phi(\boldsymbol{x})\|_{\boldsymbol{x}=\boldsymbol{x}_\odot} \\ &= R_\odot \|\nabla\Phi_{\rm B}(\boldsymbol{x})\|_{\boldsymbol{x}=\boldsymbol{x}_\odot} + G\frac{M_{\rm DM}(R_\odot)}{R_\odot}, \end{aligned} \tag{21}$$

where Φ is the total potential, Φ_B is the potential generated by the three barionic components and $M_{\rm DM}(r)$ was defined in Eq. (10). We have used the spherical symmetry property of the DM distribution in order to relate the acceleration with the enclosed mass.

A second step is to integrate the orbit forwards and backwards in time during a time interval of $\Delta t = 0.2$ Gyr, starting in both cases from a given initial condition for the progenitor. In the next sections we will explain how this initial condition was chosen for some simulations and fitted for others. The integrator used is a Runge-Kutta of order eight (`DOP853` called from SciPy's `solve_ivp` function) with relative and absolute tolerance parameters respectively given by `rtol`$= 5\times10^{-14}$ and `atol`$= 0.5\times10^{-14}$.

After having the stream's orbit integrated, we transform the orbit to both the ICRS and the GD-1 frame of coordinates. For the latter we used the `GD1Koposov10` class defined in the Gala package (Price-Whelan 2017; Price-Whelan et al. 2020) which uses the transformation matrix defined by Koposov et al. (2010). After these two transformation we obtain the orbit expressed in the observable variables (ϕ_1, ϕ_2, D, v_h, $\tilde{\mu}_\alpha$, μ_δ) used in Eqs. (1)-(6). Finally, we build interpolators of these variables as a function of ϕ_1 that will be used, together with the observed data defined in Sec. 2.1, to evaluate the following χ^2 stream function:

$$\chi^2_{\rm stream} = \chi^2_{\phi_2} + \chi^2_D + \chi^2_{v_h} + \chi^2_{\tilde{\mu}_\alpha} + \chi^2_{\mu_\delta}, \tag{22}$$

$$\chi^2_\eta = \frac{1}{\sigma^2_\eta}\sum_{i=1}^{100}\left(\eta^{(i)} - \eta(\phi_1^{(i)})\right)^2, \tag{23}$$

where η represents each of the four corresponding independent variables (ϕ_2, D, v_h, $\tilde{\mu}_\alpha$, μ_δ) and σ_η is the average dispersion of the stream data points taken by ocular inspection from Figs. 1,3,4 of Ibata et al. (2020): $\sigma_{\phi_2} = 0.5°$, $\sigma_D = 1.5$ kpc, $\sigma_{v_h} = 10$ km/s and $\sigma_{\tilde{\mu}_\alpha} = \sigma_\delta = 2$ mas/yr. Thus $\chi^2_{\rm stream}$ measures the departure of the model from the stream observations. For some fits we will also consider the departure of the model from a mass constraint in the core of the distribution:

$$\chi^2_{\rm core} = \frac{(m - m_{\rm core})^2}{\sigma^2_m}, \tag{24}$$

where $m_{\rm core}$ was defined in Sec. 2.1 and σ_m was tested between 10% and 50% of $m_{\rm core}$, so sometimes we will use the following compound function:

$$\chi^2_{\rm full} = \chi^2_{\rm stream} + \chi^2_{\rm core}. \tag{25}$$

2.4. Optimization algorithms

Our objective consists in fitting our MW model by minimizing the χ^2 function given by Eqs. (22,25). In order to do so we use two optimization algorithms for different purposes that will be explained in Sec. 3 One of them is SciPy's `optimize.differential_evolution` algorithm. This genetic architecture was used with metaparemeters given by `strategy="best2bin"`, `maxiter`=100, `popsize`=50, `tol`$=5\times10^{-8}$ and `atol`=0. This method can be run in parallel with shared memory, so a convergence test was made in a cluster's node with 24 processors, varying the values of the metaparameters (e.g. doubling the values of `maxiter` and `popsize`, setting `strategy="best1bin"` and combinations).

The other algorithm is NLopt's `LN_NELDERMEAD` called from a Julia (Bezanson et al. 2017) environment. We used default values for the all its metaparameters except for `reltol`$=5\times10^{-5}$.

3. Results

Initially, we searched for a good enough initial condition (IC) of the progenitor orbit for our Fermionic-MW. For that, we fitted the initial conditions in the (fixed) NFW-MW model defined in Sec. 2.3 by using the $\chi^2_{\rm stream}$ function defined in Eq. (22) and the genetic algorithm specified in Sec. 2.4. This IC is not uniquely determined as any point along the stream is equally good, but we just need one solution. The IC found is given by approximately by $\alpha = 149.4°$, $\delta = 36.8°$, $D = 7.9$ kpc, $\tilde{\mu}_\alpha = -7.1$ mas/yr, $\mu_\delta = -12.5$ mas/yr and $v_h = -17.3$ km/s. The corresponding orbit is displayed in the observable space in Figs. 1 and 2 with a dashed (yellow) line.

4. Discussion

5. Conclusions

Acknowledgements. Thank to people, institutions and codes used.

References

Argüelles, C. R., Mestre, M. F., Becerra-Vergara, E. A., et al. 2022, MNRAS, 511, L35
Argüelles, C. R., Krut, A., Rueda, J. A., & Ruffini, R. 2018, Physics of the Dark Universe, 21
Astropy Collaboration, Price-Whelan, A. M., Lim, P. L., et al. 2022, apj, 935, 167
Astropy Collaboration, Price-Whelan, A. M., Sipőcz, B. M., et al. 2018, AJ, 156, 123
Astropy Collaboration, Robitaille, T. P., Tollerud, E. J., et al. 2013, A&A, 558, A33
Becerra-Vergara, E. A., Argüelles, C. R., Krut, A., Rueda, J. A., & Ruffini, R. 2020, A&A, 641, A34
Becerra-Vergara, E. A., Argüelles, C. R., Krut, A., Rueda, J. A., & Ruffini, R. 2021, MNRAS, 505, L64
Bezanson, J., Edelman, A., Karpinski, S., & Shah, V. B. 2017, SIAM review, 59, 65
de Boer, T. J. L., Belokurov, V., Koposov, S. E., et al. 2018, Monthly Notices of the Royal Astronomical Society, 477, 1893
GRAVITY Collaboration, Abuter, R., Amorim, A., et al. 2018, A&A, 615, L15
Harris, C. R., Millman, K. J., van der Walt, S. J., et al. 2020, Nature, 585, 357
Ibata, R., Thomas, G., Famaey, B., et al. 2020, The Astrophysical Journal, 891, 161
Klein, O. 1949, Rev. Mod. Phys., 21, 531
Koposov, S. E., Rix, H.-W., & Hogg, D. W. 2010, The Astrophysical Journal, 712, 260
Malhan, K. & Ibata, R. A. 2019, MNRAS, 486, 2995
Malhan, K., Ibata, R. A., Goldman, B., et al. 2018, Monthly Notices of the Royal Astronomical Society, 478, 3862
Merafina, M. & Ruffini, R. 1989, A&A, 221, 4
Pouliasis, E., Di Matteo, P., & Haywood, M. 2017, A&A, 598, A66
Price-Whelan, A., Sipőcz, B., Lenz, D., et al. 2020, adrn/gala: v1.3
Price-Whelan, A. M. 2017, The Journal of Open Source Software, 2
Price-Whelan, A. M. & Bonaca, A. 2018, The Astrophysical Journal Letters, 863, L20
Schönrich, R., Binney, J., & Dehnen, W. 2010, Monthly Notices of the Royal Astronomical Society, 403, 1829
Tolman, R. C. 1930, Phys. Rev., 35, 904
Van Rossum, G. & Drake Jr, F. L. 1995, Python tutorial (Centrum voor Wiskunde en Informatica Amsterdam, The Netherlands)
Virtanen, P., Gommers, R., Oliphant, T. E., et al. 2020, Nature Methods, 17, 261

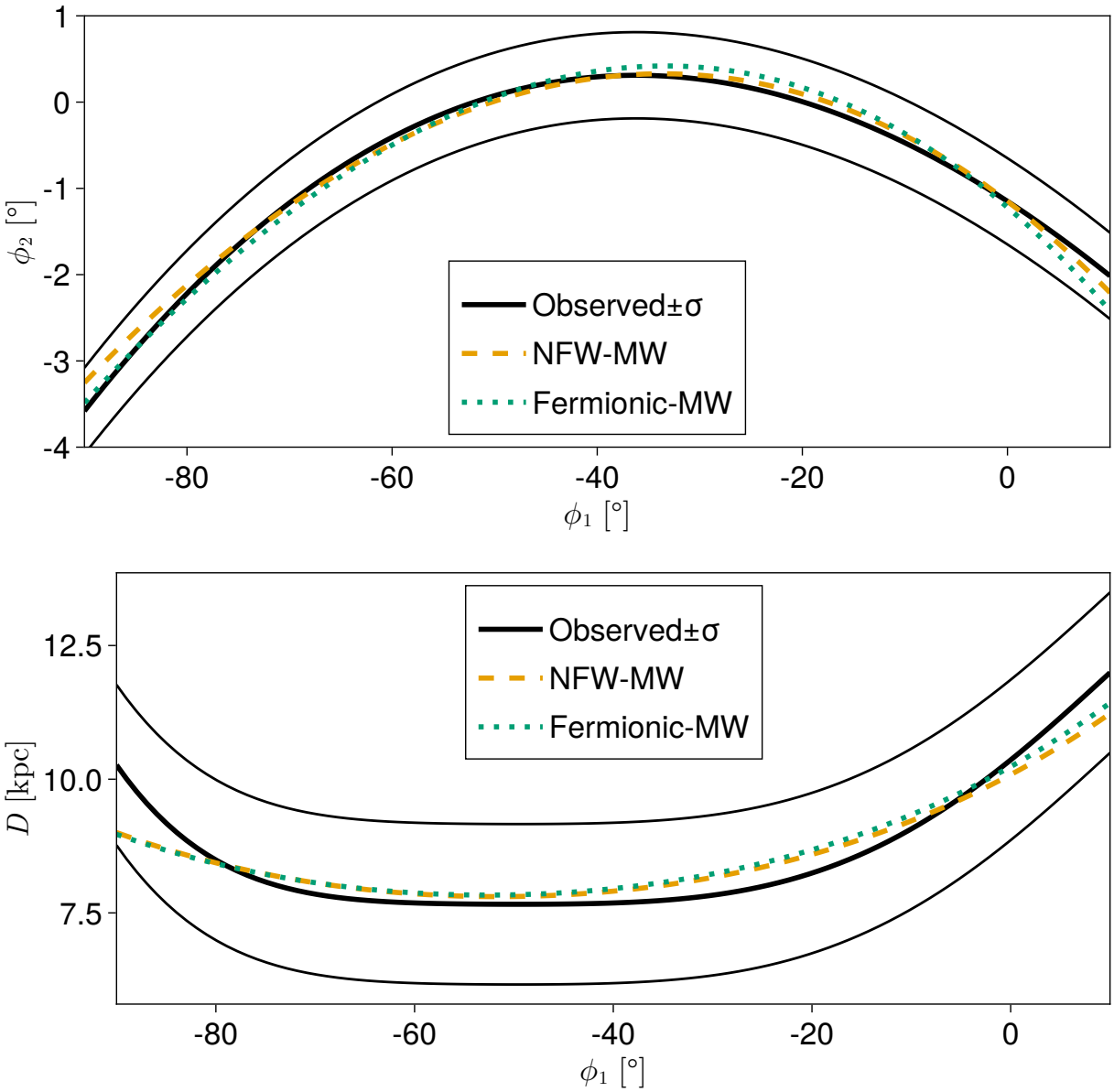

Fig. 1. Stream fits in observable space: sky position (top) and heliocentric distance (bottom).

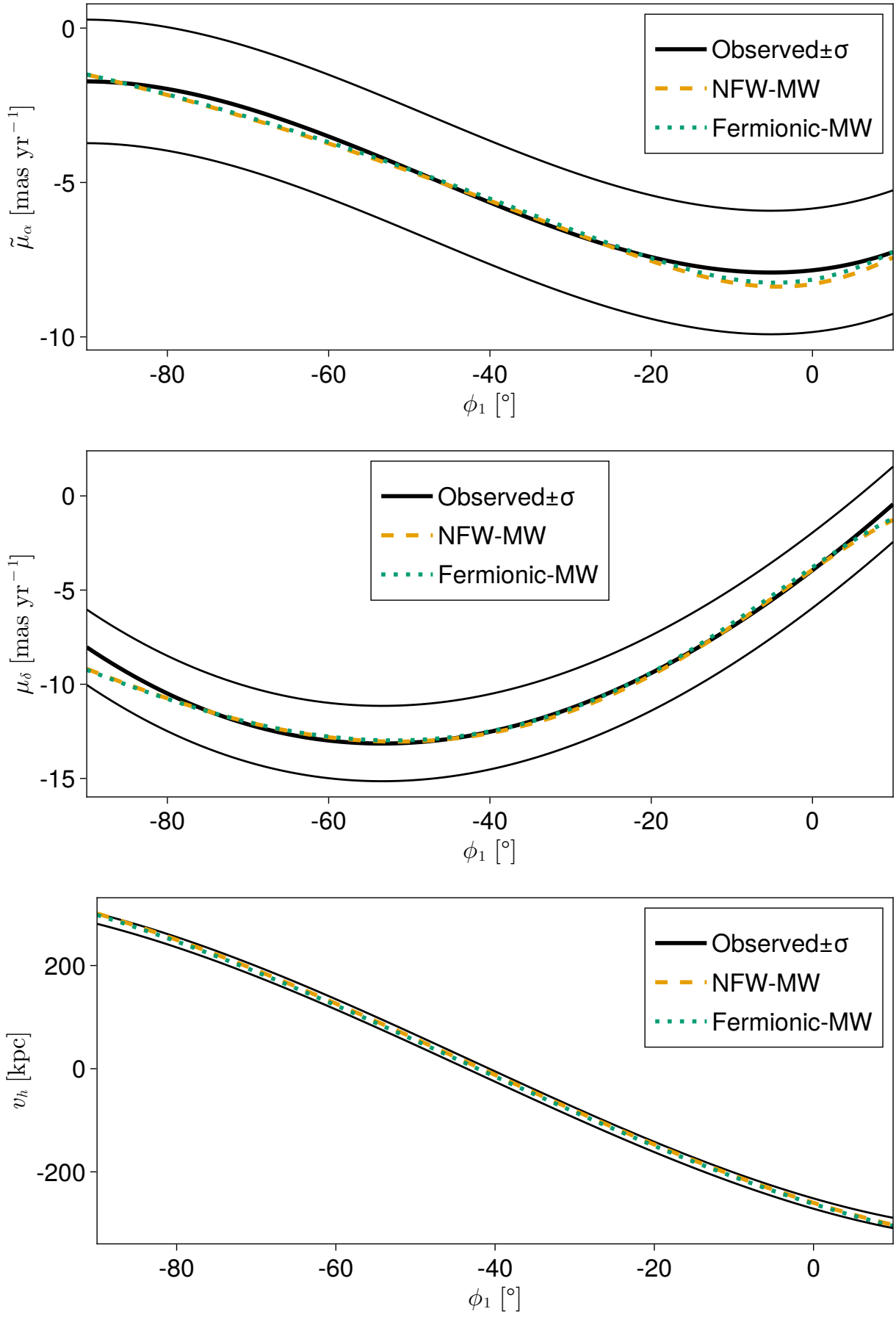

Fig. 2. Stream fits in observable space: proper motion (top-middle) and heliocentric velocity (bottom).